Experimental comparison of turbulence modulation transfer function and aerosol modulation transfer function through the open atmosphere

I. Dror and N. S. Kopeika

Department of Electrical and Computer Engineering, Ben-Gurion University of the Negev, Beer-Sheva, Israel 84105

Received February 1, 1994; revised manuscript received December 5, 1994; accepted December 14, 1994

Although turbulence is usually considered to be the primary cause of image blur, simultaneous and independent measurements of overall atmospheric modulation transfer function (MTF) and turbulence MTF over fairly long horizontal paths at 15-m average elevation indicate that, even at midday, aerosol MTF deriving from forward scatter is usually more dominant than turbulence MTF. Three different experimental techniques are used, two passive and one active. Aerosol MTF measurements are accompanied by actual meteorological and coarse aerosol size distributions and scattering parameters at the times of MTF measurements. The wavelength dependence of aerosol and therefore of overall atmospheric MTF can be significant. This wavelength dependence and a usually well-defined knee can in no way be due to turbulence but can be explained by a significant aerosol MTF deriving from typical aerosol size distributions representative of other climates as well. Measurements confirm that the narrower the open-atmosphere aerosol scattering patterns and the greater the scattering densities, the greater the degradations of aerosol MTF and, consequently, of overall atmospheric MTF. Results imply that system design and image-restoration algorithms based on atmospheric turbulence only may often lead to image quality that is much poorer than if aerosol MTF is considered, too, with its proper proportional effect on imaging through the atmosphere. Whereas adaptive optics cannot correct for aerosol-derived blur, digital image restoration can.

Key words: atmospheric optics, modulation transfer function, aerosols, scattering, turbulence, image restoration, adaptive optics.

1. INTRODUCTION

Turbulence gives rise to small-angle random tilt of the wave front, of the order typically of tens or hundreds of microradians.[1] Over a long exposure, image irradiance over many such small angles of arrival is integrated to form the recorded image, thus giving rise to image blur. Even over an exposure sufficiently short that there is time for only one angle of incidence, that angle of incidence may vary spatially over the receiver aperture, thus giving rise to blur described by the short-exposure turbulence modulation transfer function (MTF), which is a function of aperture diameter.[2] Because of such small values of wave-front tilt, long-exposure turbulence MTF recorded in the image is essentially independent of instrumentation.[1] Both the refractive-index structure coefficient C_n and turbulence MTF exhibit very weak wavelength dependencies over visible and near-infrared wavelengths.

Aerosols, on the other hand, scatter and diffuse incident light over a tremendously broad range of angles and are often modeled as being out to the diffraction limit of λ/a, where λ is wavelength and a is particulate radius.[3,4] Figure 1 illustrates schematically both the wave-front tilt caused by turbulence and the broad diffusion caused by particulate scatter that occur for radiation from a point object (spatial delta function). The diffraction limit λ/a for light scatter from aerosols is typically of the order of radians. Image-system fields of view are typically of the order of milliradians or tens of milliradians. Therefore much of the light actually scattered by aerosols is not incident upon the image sensor and thus gives rise to attenuation. However, small-angle scatter is incident and, if recorded in the image, gives rise to blur, since light from the same object point is incident upon the imager from different angles of arrival and at different positions in the image plane. An example with which many people are familiar is searching for the nighttime Moon through binoculars. An observer who moves the binoculars in the direction of increasing intensity of scattered moonlight will find the moon. This is true even for clean air, and in haze is even more so. The angular distance of the scattered moonlight seen through the binoculars can be quite extensive. Such aerosol scattered light does not exhibit the time dynamics of turbulence, but the light diffusion does give rise to very significant blur described by the aerosol MTF. The classical aerosol MTF models[4,5] did not consider effects of instrumentation in limiting the angles of arrival of received scattered light. The optical instrumentation with its limited field of view improves the quality of the image through the truncation of the scattering pattern that can affect the image, reducing the relevant angles of light scatter actually received by the imager to milliradians rather than the λ/a rad of scattered-light transmission. The image sensor affects the aerosol MTF through an additional parameter, and that is dynamic range. In the above example of observing the nighttime Moon through binoculars, much of the scattered moonlight will disappear in clear weather if part of the Moon is within the field of view. The reason is that the dynamic range of the human visual system is limited and removes the weaker-intensity scattered light from the scene because of the higher-intensity

0740-3232/95/050970-11$06.00

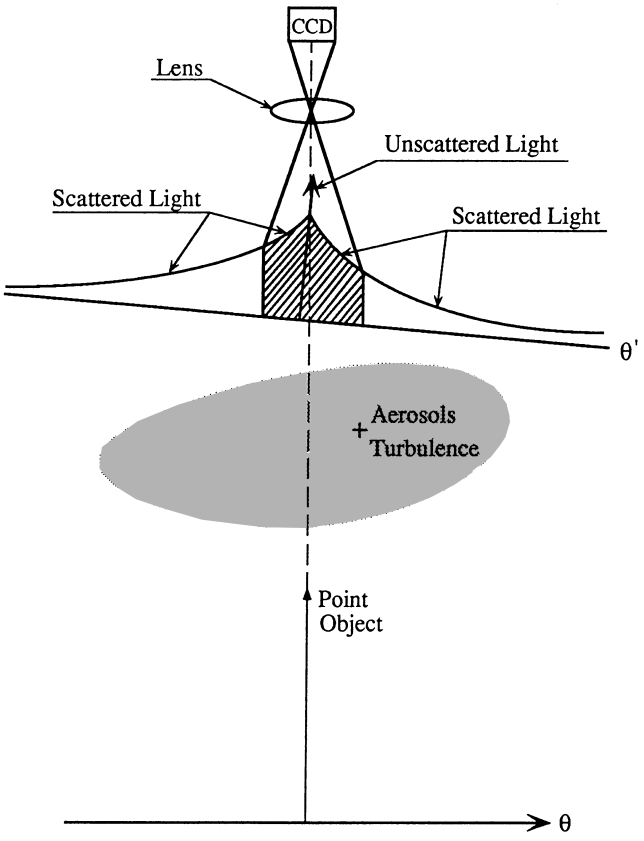

Fig. 1. Effects of aerosols, turbulence, and optics field of view on the image of the point object.

unscattered light. For this reason, if one observes a clear nighttime sky without binoculars, it will be difficult to see the scattered moonlight because the unscattered moonlight is within the field of view. With reference to Fig. 1, this means that not necessarily all the scattered light from the point object that is within the field of view and incident upon the sensor is actually recorded in the image. The received radiation deriving from larger angles of light scatter is of lower intensity than that deriving from smaller angles of light scatter. Hence the dynamic range of the imager of the scene itself may truncate the received scattered light at scatter angles of the order of tens or hundreds of microradians, which are smaller than the field of view shown in Fig. 1. It is such small-angle scatter, rather than the larger-angle scatter that is truncated by the instrumentation, that blurs the image. The optics and sensor instrumentation effects give rise to a practical instrumentation-based aerosol MTF that describes the aerosol MTF that actually affects the image,[6] rather than the classical aerosol MTF at the optics input that describes blur that would take place at larger scatter angles were it not for such truncation by the instrumentation.

The atmospheric angular point-spread function (PSF) recorded in the image consists of a narrow component representing the unscattered light and a lower very broad component representing the scattered light. The unscattered light input to the optics is an angular delta function, and it gives rise to a constant MTF component out to infinite spatial frequency in the angular spatial-frequency domain. For an infinite instrumentation spatial-frequency bandwidth, it would give rise to an unblurred image. Therefore some blurring occurs as a result of the spatial-frequency bandwidth of the optics and particularly of the sensor. The scattered-light component of the PSF, or the specific-intensity function, gives rise to a blurred image described by the scattered-light MTF component in Fig. 2. The angular cutoff spatial frequency Ω_c describes the limitation of received scatter angles derived from field-of-view or dynamic-range limitations, whichever limit is smaller. The smaller the angles of light scatter recorded in the image (spatial domain), the larger is Ω_c in the spatial-frequency domain and the sharper is the image. The value of Ω_c derived from the instrumentation is therefore orders of magnitude higher than the value of a/λ expected from the classical aerosol MTF at the optics input. (Aerosol MTF calculations by Zege[7] *et al.* and by Bissonnette[8] did not consider effects of instrumentation[6] in limiting light scatter angles actually recorded in images. They considered aerosol MTF only at the input to the optics instrumentation rather than that recorded in the image. Hence their calculations exhibit Ω_c of the order of only a/λ.)

Therefore the aerosol MTF describes a superposition of two images: an essentially (but not totally) unblurred image deriving from received unscattered light and a blurred image deriving from received scattered light, where, for small optical depths, angles of light scatter actually recorded in the latter image are limited almost always by instrumentation field of view or dynamic range or by object-scene dynamic range. In the unscattered-light image there is some limited blur resulting from limited spatial-frequency bandwidth of the instrumentation, which widens line-spread functions (LSF's) and PSF's from delta functions, thus causing some blur. This is illustrated here in results shown in specific-intensity plots (Figs. 8, 10, and 12 below). In the scattered image, instrumentation limitations to angles of light scatter actually recorded in the image increase Ω_c from cycles per radian to cycles per milliradian or more, depending on instrumentation and scene parameters. This is also illustrated in the specific-intensity plots. Scattering processes and aerosol MTF are very strongly wavelength dependent according to the ratio of a/λ, whereas turbulence MTF exhibits very weak improvement at longer wavelengths.

In general, the quality of images propagating through an atmospheric path are degraded by a number of atmospheric phenomena. The degradation in the image plane

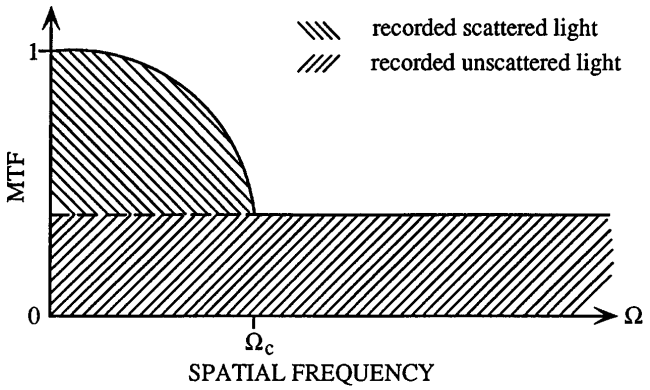

Fig. 2. Simplified aerosol MTF (after Ref. 9).

at the receiver can be quantified by the overall atmospheric MTF. Each of the atmospheric degrading effects has it own MTF. If the atmospheric MTF's are uncorrelated the overall atmospheric MTF can be written as the product of the MTF components[3,4]:

$$M_A = M_a M_T , \tag{1}$$

where M_a is the practical aerosol MTF[6] and M_T the atmospheric turbulence MTF.[2,10] Both small-angle random scattering by aerosols and small-angle random refractions by turbulence cause blurring but by different mechanisms, as explained above. The aerosol scattering diffuses and broadens the object beam. Turbulence causes wave-front tilt that is integrated over many angles of incidence during long exposure time. In system design it is important that one consider the origin of atmospheric blur in order to minimize it and correct for it. Often turbulence has been assumed to be the primary or even the only source of atmospheric blur. In this paper are presented simultaneous and independent comparisons of aerosol and turbulence MTF. Aerosol MTF is observed to be always significant[11] and often more dominant than turbulence MTF except at midday. This means that imaging-system design and image-restoration algorithms based primarily on turbulence are often not going to be too effective, since they do not take into account aerosol-related blur. However, image-restoration algorithms based on both turbulence and aerosol MTF can be extremely effective in deblurring atmospheric blur, particularly if the unique shape of aerosol MTF in Fig. 2 and the high value of Ω_c are considered. In such cases atmospheric blur can be removed essentially completely.[12]

The ability to predict atmospheric MTF can permit prediction of image quality under various meteorological conditions. If the prediction is accurate and reliable it can be used also to restore the blurred image and to recover some of the fine details. It has been shown[13] for a specific situation that the atmospheric MTF for horizontal visible and near-infrared optical paths can be predicted directly from standard macroscale meteorological parameters, such as temperature, relative humidity, and wind speed, that are available from a standard meteorological station.

A more general approach can involve separate forecasts of aerosol and turbulence MTF's and then multiplication of the two predicted MTF's if they are independent. The benefit of this approach is that the atmospheric MTF can be predicted from the basic weather parameters that are responsible for image degradation. Atmospheric-turbulence strength along horizontal imaging paths is related statistically to simple standard macroscale weather parameters,[14] so the turbulence MTF can be deduced from standard meteorological quantities. This has been verified in experiments in both Israel and France,[14,15] the latter experiments carried out by the U.S. Army Night Vision Laboratory. LOWTRAN, MODTRAN, and other models suggest that aerosol statistics, distribution, and distribution parameters can also be deduced from such macroscale parameters.[16,17] Since particulate distributions are predictable by macroscale meteorological quantities, it is possible to reconstruct the aerosol MTF from these data. The absorption, A_a, and the scattering, S_a, coefficients and the phase functions of particulates needed for modeling the aerosol MTF can be calculated from a known particulate distribution and from the refractive index of particles by Mie scattering theory.[18] For larger optical densities, multiple-scattering techniques may be used.

As part of this experimental program to predict overall atmospheric MTF, separate measurements were carried out concerning turbulence MTF and overall atmospheric MTF. Generally, the atmospheric resolution limit is popularly associated with turbulence. In these measurements the effect of aerosols in limiting resolution through the atmosphere was often much more noticeable than that of turbulence. First are described three separate methods by which overall atmospheric MTF was measured. Each method has advantages and disadvantages. This is followed by a description of turbulence MTF measurements and extraction of aerosol MTF data. Included, too, are aerosol size distribution and meteorological measurements at the time of atmospheric and turbulence MTF measurements. As discussed below, laboratory aerosol MTF measurements have in the past been associated only with aerosols of uniform size. Here, aerosol MTF measurements are presented for the open atmosphere and are accompanied by measurements of actual coarse aerosol size *distribution* and weather data at the times of the MTF measurements. The three methods from which aerosol MTF is extracted yield very similar results concerning aerosol MTF shape as well as the significance of aerosol MTF relative to turbulence MTF. Two of the methods involve measurements of turbulence and overall atmospheric MTF over the same pixels. All three methods involve simultaneous and independent measurements of turbulence and overall atmospheric MTF. This permits aerosol MTF determination through Eq. (1).

2. EXPERIMENT

A. Atmospheric Modulation Transfer Function Measurements

Measurements of the atmospheric MTF were taken through three experimental techniques. The first two methods use the passive light pattern of sunlight reflected from black and white stripes on a resolution chart. The third method involves imaging of a laser beam serving as a point source. The imaging system consists of a Questar telescope with 89-mm aperture diameter and 1400-mm focal length, Barlow lens, filters, and a silicon CCD video camera connected to a frame grabber mounted in a personal computer. Spectral response of the optics and the CCD is over the wavelength range of approximately 300–1000 nm. The imaging system is controlled by the computer, which is also responsible for the data analysis. The light pattern observed at the image plane depends on the method used for measuring the atmospheric MTF.

The first method is derived from the bar chart contrasts. The object plane, 5.5 km northward from the imaging system, consisted of a resolution bar chart composed of vertical black and white line pairs of varying spatial width. Average elevation of line of slight was approximately 15 m. Each vertical line pair represents a different angular spatial frequency. Resolution was such that 10-cm-wide lines were easily distinguishable in clear

weather over the 5.5-km horizontal path length. We detected the edges of each bar image by taking the derivative of the Gaussian low-passed[19] bar image over each of 80 horizontal video lines. This was important because the edges of the resolution chart image tended to wander as a result of the fluctuations in ray angles of arrival caused by atmospheric turbulence, especially when this effect was extreme. Spatial-frequency response was isolated from the individual video line. The black and white square-wave responses were Fourier transformed, and only the first harmonic of the square-wave response, representing the sine-wave image response, was taken. This value, after proper normalization, is the spatial-frequency response of the atmosphere and the imaging-system combination at each specific spatial frequency. For more accuracy the method was repeated over 80 horizontal video lines from the center of the resolution chart, and the responses were averaged. In this way overall atmospheric MTF measurements were obtained and repeated under different meteorological conditions and with different high-pass optical wavelength filters over visible and near-infrared wavelengths.

The second method was based on the image of a sharp vertical *edge* separating 2-m-wide black and white bars, which composed the lowest spatial frequency of the bar chart. In each of the MTF measurements, 20 sequential exposures were taken. Each exposure contains simultaneously 80 different horizontal video lines from the edge response. All the horizontal video lines that describe the atmospheric vertical-edge response were added to a single-edge response. Even if each 1/60-s exposure were considered to be a short exposure involving only one angle of tilt (and this is doubtful since generally short exposure should involve at most 1 ms of exposure time), the adding of 20 such exposures where each contains 80 video line responses can be considered generally to be representative of a long exposure. The LSF was calculated from the edge response by isolation of the monotonic part of the average edge response, and noise was rejected by use of a recursive nonlinear smoothing algorithm,[20] with the derivative then being taken. Overall MTF was calculated by expansion of the LSF with additional zeros and Fourier transformation of the expanded LSF by the fast-Fourier-transform algorithm. The MTF measurements were repeated under different meteorological conditions and with different high-pass optical wavelength filters over visible and near-infrared wavelengths. Reflectance measurements indicated that the black and white painted bars were spectrally neutral over 425–1100-nm wavelength (Fig. 3). With this method turbulence and atmospheric MTF were measured simultaneously and independently over the same pixels. The method for measuring turbulence MTF is described in Subsection 2.B.

In the third and active method the light pattern of a distant He–Ne laser serving as a point source was observed. The He–Ne laser beam was imaged into the image plane. A narrow-band interference filter was used, improving the ratio of the laser intensity image in the image plane to the background illumination. This made possible the measurement of atmospheric PSF even under daylight conditions. The overall MTF of the atmosphere and the imaging system is simply the two-dimensional Fourier transform of the recorded PSF. In this third and active method, the separation between the imaging system and the laser source was 6.2 km. Experience has shown that even over shorter path lengths in colder climates, laser beam coherence is rather completely destroyed at the visible wavelengths,[21] so these measurements were considered from the standpoint of incoherent radiation. Also, coherence diameter in the aperture plane was almost always less than 1 cm, according to the e^{-1} value of the mutual coherence functions corresponding to measured overall atmospheric MTF's. Since the aperture diameter was 8.9 cm, coherence area generally was only ≈1% of the aperture area. Hence coherence effects are negligible here. The measurements were taken at Ben-Gurion University of the Negev during the summer of 1991. In this third method, too, the measurements of overall atmospheric and turbulence MTF's were simultaneous and independent and over the same pixels. Weather measurements were on line with a computerized weather station near the imaging system.

The coarse aerosol distribution was also measured over the radius (r) range 0.16–10 μm with CSASP-100 instrumentation manufactured by Particle Measurements Systems (PMS), Inc. Comparisons[22] of atmospheric transmission according to the PMS instrumentation measurement with atmospheric transmission measured with black target–sky luminance contrast[23,24] carried out over the same experimental path indicate that the contribution of the fine aerosols ($r < 0.16$ μm) to the scattering coefficient at 0.5-μm wavelength is small (≈10%) in haze and is more significant (≈50%) in clear weather. If MODTRAN models of the fine aerosols are considered too, calculations indicate that overall scattering diagrams hardly change, whereas scattering coefficients at shorter wavelengths are increased by the addition of fine particulates slightly more than are those at longer wavelengths. In general, the distribution of fine aerosols changes little with weather even from clear weather to sandstorms, whereas that of the coarse aerosols varies significantly even in clear weather and depends greatly on humidity. In the climate in which our experiments were conducted, relative humidity is usually high in the early mornings and evenings and low during much of the day. Hence, coarse aerosol size distributions often change noticeably

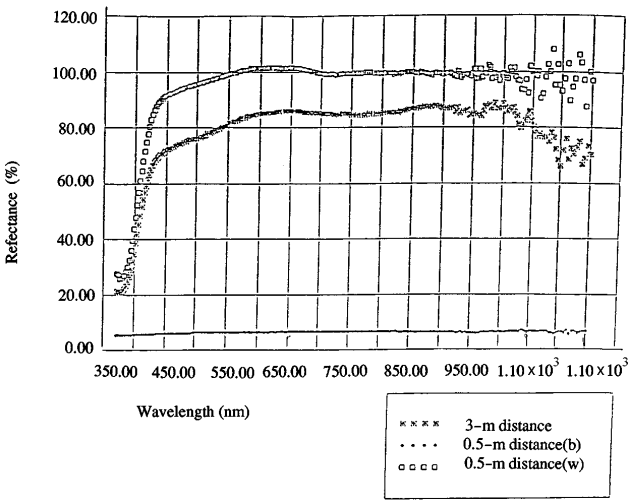

Fig. 3. Spectral response of the bar chart.

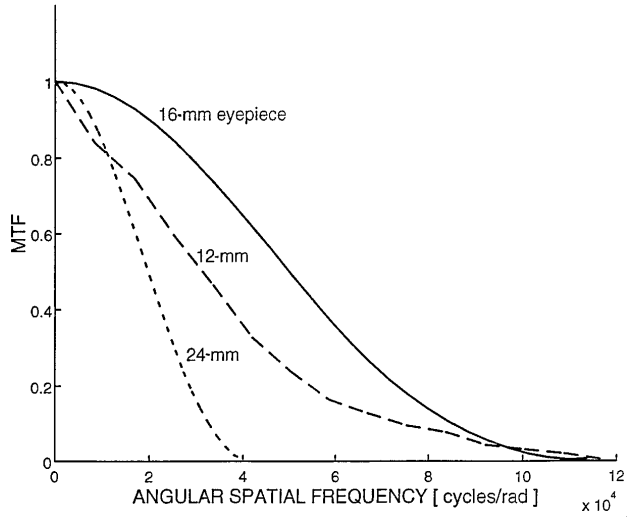

Fig. 4. Imaging-system MTF for three different eyepieces.

during the course of a day, as do the extinction coefficients and the scattering diagrams. These data are included here as well. Although the coarse aerosol data were measured directly with the PMS instrumentation, extrapolations were made with use of MODTRAN to include the small aerosols, whose distribution varies little with weather.

The MTF of the imaging system was also measured. This MTF is composed of degradations by the optical lens, the CCD camera, and the frame grabber. Figure 4 describes the imaging-system MTF for three different eyepieces. Since the best performance was achieved with a 16-mm eyepiece, this eyepiece was chosen. Hardware MTF is seen to extend beyond 100 cycles/mrad. Field of view was limited to 1.9 mrad. The overall atmospheric MTF was calculated by division of the total measured MTF by that of the imaging system, because the degrading effects of the system and the atmosphere are independent of each other. The atmospheric MTF was normalized to unity.

B. Turbulence Modulation Transfer Function

In order to measure the aerosol MTF, we made measurements of atmospheric turbulence simultaneously and independently over the same atmospheric optical path. The first two experimental setups, which are passive, also include turbulence measurements by an edge-wander technique.[11] The imaged edge used in this experiment was the same vertical-separation edge between black and white bars. The turbulence measurement was based on angle-of-arrival variance. The rms horizontal angles of arrival of sunlight reflected from the edge were calculated. The same images and 80 video lines per image used to determine the LSF were used also to determine C_n^2. The relationship between overall beam mean-squared one-dimensional angle of arrival and the refractive-index structure coefficient is given by[25]

$$\langle \alpha_x^2 \rangle \approx 2.92 D^{-1/3} \int_0^L C_n^2(z) \left(\frac{z}{L} \right)^{5/3} \mathrm{d}z, \qquad L_0 > D \gg (\lambda L)^{1/2}, \quad (2)$$

where α_x is the horizontal component of angle of arrival in radians, D is the aperture diameter, L is the length of the atmospheric path, and C_n^2 is refractive-index structure coefficient. L_0 is the outer scale of the turbulent eddies. In our experiments $D = 89$ mm, which is larger than $(\lambda L)^{1/2}$. The results of this passive near-field technique involving reflected sunlight for measuring C_n^2 showed excellent agreement with an active method for measuring atmospheric turbulence according to amplitude fluctuations of a CO_2 laser beam in which the Rytov approximation was measured experimentally to hold.[14] Hence the use of relation (2) for edge wander is justified on the basis of experimental comparison involving also three different methods with which to measure C_n^2 (Ref. 14). It should be made clear that this technique does not involve measurements of blur, which would involve aerosol MTF as well, but only edge wander of the line separating the widest bar pair in the scene. The MTF of atmospheric turbulence for long exposures is given by[2,10]

$$M_T = \exp\left[-57.53 \Omega_r^{5/3} \lambda^{-1/3} \int_0^z C_n^2(z) \left(\frac{z}{L} \right)^{5/3} \mathrm{d}z \right], \quad (3)$$

where Ω_r is angular spatial frequency and λ is wavelength.

The third and active atmospheric MTF measuring method includes the measurement of turbulence by measurement, in all directions, of the beam wander of a He–Ne laser beam.[10,26]

In both the second and the third methods, overall atmospheric MTF and turbulence MTF were measured simultaneously and independently over the same portion of the same images, the former from LSF or PSF and the latter from angle-of-arrival variance. The first method involved independent and simultaneous measurements of overall atmospheric and turbulence MTF's but over different portions of the image. Nevertheless, the results with all these methods were quite similar.

The first and the second techniques involve edge wander of a long vertical stripe. For long horizontal paths, as in these experiments, isoplanatic size is very small, often less than a single video line.

The isoplanatic angle is usually defined according to[27]

$$\theta_0 = \left[2.91 k^2 \sec^{8/3} \phi \int_0^L C_n^2(z) z^{5/3} \mathrm{d}z \right]^{-3/5}, \quad (4)$$

where for imaging upward ϕ is the angle from the zenith. Typical values of θ_0 for imaging upward are of the order of several microradians, as summarized by Beland,[25] and increase for strong turbulence. For a horizontal path, and assuming a fairly homogeneous atmosphere so that n^2 is a path integrated average, Eq. (4) is simplified to

$$\theta_0 = \left(\frac{3}{8} 2.91 k^2 C_n^2 L^{8/3} \mathrm{d}z \right)^{-3/5}. \quad (5)$$

Assuming a representative wavelength of 0.5 μm and a horizontal path length of 5.5 km, θ_0 is calculated to be of the order of 0.2 μrad for strong turbulence ($C_n^2 = 10^{-13}$ m$^{-2/3}$) and 3 μrad for weak turbulence

($C_n^2 = 10^{-15}$ m$^{-2/3}$). Corresponding isoplanatic patches in the object plane are therefore of the order of 1 mm in strong turbulence and 1.64 cm in weak turbulence. Since field of view is 1.9 mrad, the scene diameter viewed is approximately 11 m. Out of 512 possible horizontal lines, the 80 video lines used for angle-of-arrival and PSF calculations correspond to an object-plane scene dimension of 1.7 m. Therefore in strong turbulence the object-scene dimension of 1.7 m considered for calculations is composed of 1.7 m/1 mm = 1700 isoplanatic patches, and in weak turbulence over the same vertical dimension there are approximately 1.7 m/1.64 cm or 104 isoplanatic patches. Since there are only 80 video lines covering this object-plane dimension, each of the 80 video lines represents a separate isoplanatic patch in both weak and strong turbulence.

Measurement of horizontal angle of arrival of a long vertical bar over 80 video lines therefore involves at least 80 different angles of arrival for each exposure. Adding 20 such exposures then involves 1600 horizontal angles of arrival. Although approximately 1600 isoplanatic patches are involved in each measurement of edge wander, the statistics of each isoplanatic patch can be expected to be the same; i.e., the angle-of-arrival variance can be expected to be the same. Hence adding more than 1600 isoplanatic patches deriving from the 80 video lines and 20 exposures is representative of a very long exposure (1600/30 = 53 s). It is conceivable that under certain weather conditions the whole bar chart image may represent a single isoplanatic patch, in which case the calculation of C_n^2 involves only an equivalent exposure length of 20/60 = 1/3 s. This may not represent an ideal long exposure, but it is much closer to a long exposure than to a short exposure even under such conditions. In any event, since the overall atmospheric MTF and the turbulence MTF were measured simultaneously over the same exposure time, the image motion temporal spectra involved in both MTF determinations are identical. In methods 2 and 3 they are also over the same pixels. Therefore, if atmospheric MTF were to derive essentially from turbulence only, the turbulence and the atmospheric MTF's should be identical for any given exposure time. Results described in Section 3 below show that they are not.

C. Aerosol Modulation Transfer Function

Aerosol MTF was obtained by division of overall measured atmospheric MTF by the measured turbulence MTF. It was assumed that turbulence MTF and particulate MTF are uncorrelated. Overall atmospheric MTF and turbulence MTF were usually found to be far from identical. Overall atmospheric MTF usually exhibited a clear knee associated with aerosol MTF as in Fig. 2. This was also observed previously[28] and cannot be explained in any way by any value of C_n^2 whatever, nor can the wavelength dependencies. Furthermore, the logarithmic slope of overall atmospheric MTF for $\Omega_r < \Omega_c$ was much more negative than the $-5/3$ slope expected from turbulence in Eq. (3).

D. Comparison of the Three Methods of Measurement

Both passive methods used a passive light pattern for observing the image blur when the light was propagating through the atmosphere. An advantage of the second, or edge-response, method over the first is that the MTF measured by the edge-response method is continuous, whereas the first method measures the MTF only at several discrete spatial frequencies according to the object-plane bar pattern. Another advantage of the second technique is that both MTF and turbulence measurements are extracted from the same pixels. This is true also in the case of the third and active method.

In a comparison of the passive methods with the active method, the active method features a very good signal-to-noise ratio. Here, as in the moonlight example of Section 1, when the receiver was pointed near the He–Ne laser beam source but the laser was not in the field of view, the field of view was filled with red light that increased in intensity as the receiver was directed closer to the direction of the laser. Once the laser was in the field of view, the red background disappeared. The narrow-band He–Ne laser filter reduces the red natural background light to levels not recorded by the imaging system because of dynamic-range limitations. Much of the scattered laser light is also not recorded in the image because of dynamic-range limitations. The active method is not limited to daylight conditions. On the other hand, the wave front transmitted from the passive bar chart is spherical, whereas the laser wave front is narrow and Gaussian. An important disadvantage is that the third method is limited to laser wavelengths. Wavelength filters with the two passive methods permitted comparison of turbulence and aerosol MTF's at various wavelength bands in the sunlight spectrum reflected from the resolution chart.

3. RESULTS

Results of the first method have been presented in detail elsewhere.[29] Here we concentrate on methods 2 and 3.

Figure 5 shows typical atmospheric MTF curves produced with the passive edge-response method (method 2) over different wavelength intervals for a summer morning. The knee evident in overall atmospheric MTF and the subsequent leveling off cannot be attributed to turbulence, nor can wavelength differences, no matter what values of C_n^2 are assumed. These types of curve showed up consistently in all three types of measurement. In each of the three experiments the edge response was taken with different optical high-pass wavelength filters. The solid curves in the figures are the normalized overall atmospheric MTF. The dotted curves are those of turbulence MTF. From relation (2) a path-integrated value of C_n^2 was obtained, and the turbulence MTF was calculated as in Eq. (3). Division of the overall atmospheric MTF by the turbulence MTF yielded the aerosol MTF, shown by the dashed curves. [The turbulence MTF curve in Fig. 5(a) is higher and the aerosol MTF curve there lower than those shown in Ref. 11. The curves there are in error because the numerical coefficient 2.92 in Eq. (2) here was applied there wrongly for two-dimensional instead of one-dimensional angle-of-arrival variance.] The aerosol MTF is seen to be dominant, particularly at shorter wavelengths. The shape of the aerosol MTF resembles very strongly in form that expected from Fig. 2, and the relatively high value of Ω_c supports the practical instrumentation-based theory of the aerosol MTF.[6]

This shape of the aerosol MTF curve has been veri-

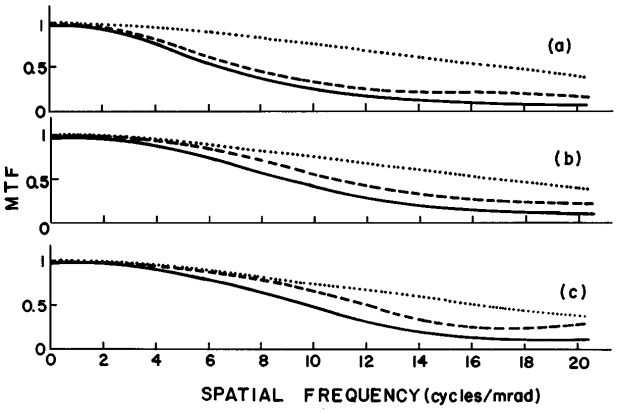

Fig. 5. Overall atmospheric (solid curves), turbulence (dotted curves), and aerosol (dashed curves) MTF's measured July 16, 1991, at 7:03 am by observation of an edge through different high-pass wavelength filters. (a) $\lambda > 280$ nm, (b) $\lambda > 530$ nm, (c) $\lambda > 715$ nm. Aerosol MTF's were obtained from the ratio of overall atmospheric MTF to turbulence MTF.

fied experimentally under controlled laboratory conditions by Kuga and Ishimaru[30] and by Donelli *et al.*[31] in which single aerosol sizes rather than distributions were used in each experiment. In our experiments, which involve polydisperse distributions of natural aerosols, and in theirs the existence of an aerosol cutoff frequency was observed clearly in almost all the measurements, even when optical density was not much less then unity. Measurement uncertainty is of the order of a pixel divided by the square root of the number of exposures. This generates an uncertainty in the angle-of-arrival variance and in the overall atmospheric MTF measurements up to $\pm 2\%$.

Figures 6, 7, and 8 show coarse aerosol distribution, scattering coefficient, and specific-intensity calculations, respectively, at representative wavelengths for the aerosol MTF measurements in Fig. 5. Weather data for all three figures are given in the caption for Fig. 6. In the specific-intensity diagrams the radiances to the left represent the unscattered light, broadened from delta functions by the limited spatial-frequency bandwidth of the sensor. The scattered-light contributions are to the right. Note that the aerosol MTF's in Fig. 5 are narrowest at shorter wavelengths. In Fig. 8 shorter wavelengths yield broader scattering diagrams and larger scattering coefficients. The scattering coefficients stemming from only coarse aerosols shown in Fig. 6 are 0.3, 0.29, and 0.28 km^{-1} at 450, 550, and 720 nm, respectively. Whereas attenuation in Fig. 7 is for coarse aerosols only, S_a in Fig. 8 includes as well extrapolation from MODTRAN for the fine aerosols at representative wavelengths. Fourier transforms of the specific intensities calculated from the aerosol size distributions and dynamic-range limitations yield aerosol MTF's similar to those measured in Fig. 5 despite the fact that the calculations are for representative discrete wavelengths, whereas the MTF measurements are over broad spectral regions, and despite the fact that the size distributions for the fine particulates are not measured but estimated. These estimates introduce some uncertainties into the values of optical depth with which to consider the MTF measurements. The dynamic-range thresholds in Fig. 8 were slightly more than 1% of the unscattered light irradiance.

The broader the scattering angles and the lower the scattering densities, the broader the aerosol and the overall atmospheric MTF's. Aerosol size distributions here are not unique and are similar to those measured elsewhere, such as in the central United States.[32] Therefore the comparison between aerosol and turbulence observed here should also be relevant elsewhere.

Similar MTF and aerosol data are shown in Figs. 6, 7, 9, and 10 for midday. Here, because it is midday, turbulence MTF is somewhat lower than in the mornings, but overall atmospheric MTF is still dominated by aerosol MTF, despite the lower humidity that reduces optical depth. The trends concerning specific intensity and aerosol MTF in Figs. 5 and 8 appear again in Figs. 9 and 10. Calculations of S_a for only the coarse aerosols in Fig. 6 are 0.146, 0.142, and 0.138 km^{-1} at 450, 550, and 720 nm, respectively. However, here too, as in the upper

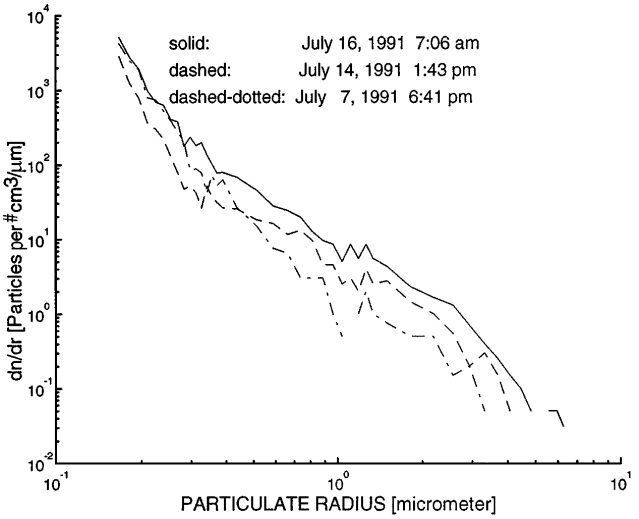

Fig. 6. Measured coarse aerosol size distributions. For July 16 at 7:06 am, air temperature was 20 °C, relative humidity was 66%, wind speed was 1 m/s, wind direction was 50 °C, and solar flux was 0.3 kW/m^2. For July 14 at midday the respective weather data were 33 °C, 39%, 5 m/s, 237 °C, and 0.95 kW/m^2. For July 7 at 6:41 pm the respective weather data were 235 °C, 59%, 5 m/s, 220 °C, and 0.027 kW/m^2.

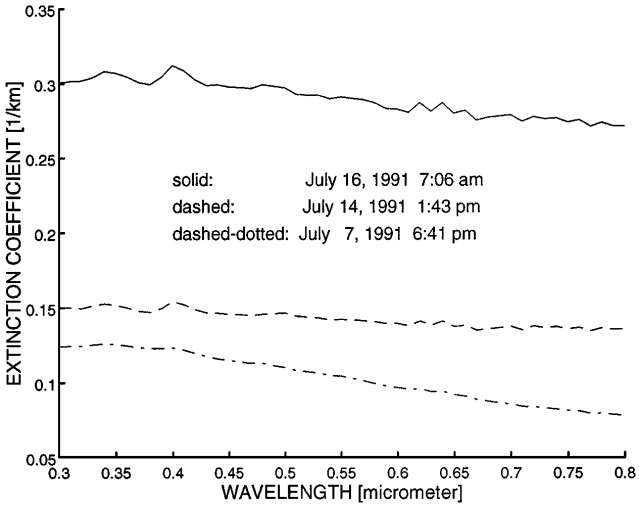

Fig. 7. Calculated scattering coefficients for coarse aerosols. Weather conditions as for Fig. 6.

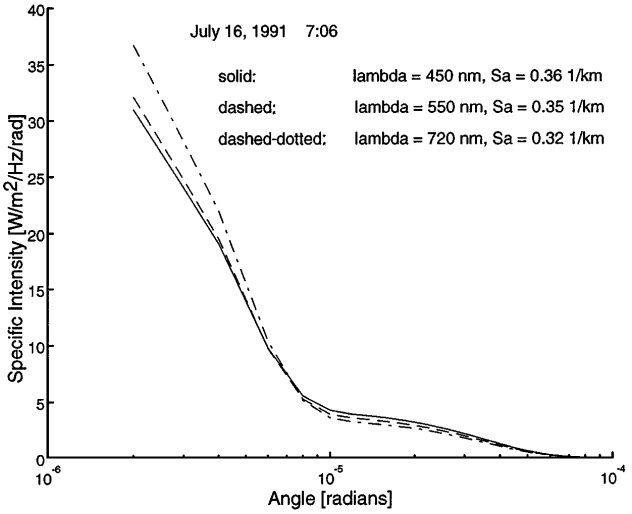

Fig. 8. Calculated specific-intensity functions with scattering coefficients for coarse and fine aerosols together for July 16 at 7:06 am. Weather conditions as for Fig. 6.

curve in Fig. 7, there are noticeable hills and valleys in the middle spectral-attenuation curve of Fig. 7 for midday, so that attenuation at the above three wavelengths is not necessarily representative of optical depth over the spectrally broad MTF measurements of Fig. 9.

Figures 6, 7, 11, and 12 show similar MTF and aerosol data from the late afternoon. Aerosol MTF is again dominant, particularly at shorter wavelengths, at which the scattering diagram is narrower and scattering density is greater. Calculations of S_a for only the coarse aerosols in Fig. 6 are 0.11, 0.1, and 0.08 km^{-1} at 450, 550, and 720 nm, respectively. Although the aerosol MTF shape in Fig. 11 is more obvious at longer wavelengths, image degradation by aerosols is less than at shorter wavelengths. In general, the late-afternoon scattering densities were less than at midday, and the late-afternoon aerosol MTF's are less significant than those of midday. However, the reduced turbulence makes the late-afternoon aerosol MTF's more obvious. The reduced scattering in the late afternoon despite the increased relative humidity may be due to temperature effects.[22]

Figure 13 shows similar data for the laser point source measurements (method 3). Aerosol MTF is clearly evident, particularly in the morning. Aerosol MTF is least evident in the midday measurement, for which the scattering diagram was broadest. It is most noticeable in the morning, when scattering density is greatest. Measurements were recorded daily over many months. Results presented here are typical.

4. DISCUSSION

The practical instrumentation-based aerosol MTF is seen at 15-m elevation to be more significant than turbulence MTF in almost every case, including at midday when C_n^2 is maximum. The shape of the aerosol MTF is seen to resemble closely that expected from theory[6] as shown in Fig. 2, where the wavelike nature for spatial frequencies higher than Ω_c derives from the spatial-frequency limitation imposed by the equipment. The measured values of Ω_c are close to theoretical predictions[6] based on the instrumentation parameters and aerosol size distributions. Since the calculations appear in Ref. 6 they are not repeated here. The method of practical aerosol MTF calculations is summarized elsewhere.[33]

There is not enough detail in the papers on the experiments of Kuga and Ishimaru[30] and of Donelli *et al.*[31] to permit us to calculate their practical aerosol MTF's. However, it is clear that values of Ω_c in their experiments are higher than a/λ.

Bissonnette measured aerosol MTF's for rain and fog[8] over short distances of 531 and 921 m. In those cases aerosol MTF was clearly dominant over turbulence MTF. Unfortunately, he was not able to measure aerosol MTF for clear weather and haze. However, in such cases he was unable to measure any atmospheric MTF whatever, including turbulence MTF. Indeed, analysis[33] of his equipment[8] indicates that his hardware MTF extended out to only 2–3 cycles/mrad, and this is way too low for measurement of any clear-weather or haze atmospheric MTF, whether it be dominated by aerosol or by turbulence MTF. In such situations his image blur derived from hardware only. The measurements reported here, on the other hand, involve equipment MTF (see Fig. 4) out to more than 100 cycles/mrad, which is almost 2 orders of magnitude greater resolution. Both tur-

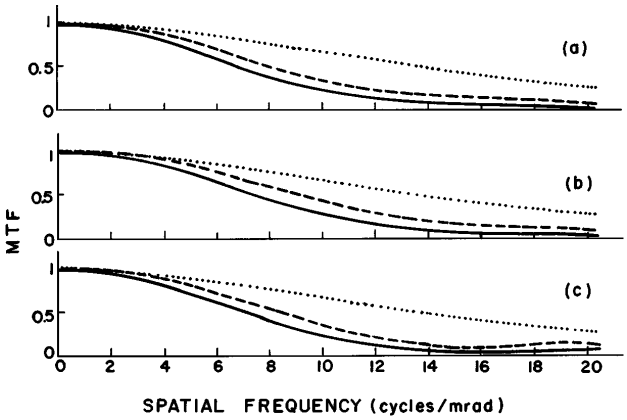

Fig. 9. Same as Fig. 5 but for July 7 at 1:42 pm; (c) is for $\lambda > 665$ nm.

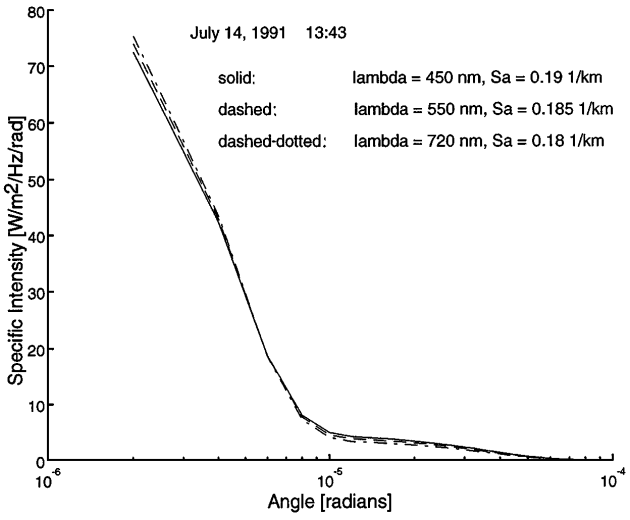

Fig. 10. Calculated specific-intensity functions with scattering coefficients for coarse and fine aerosols together for July 7 at 1:42 pm.

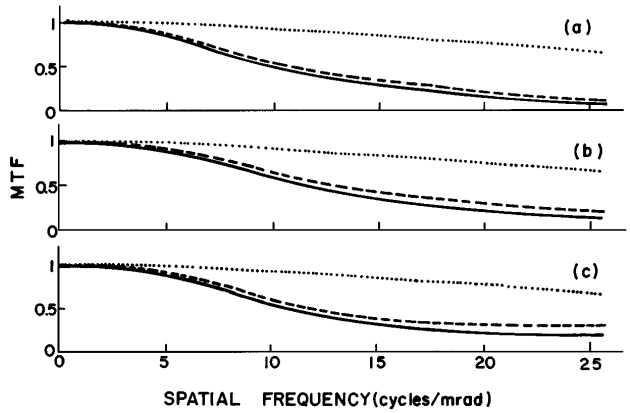

Fig. 11. Same as Fig. 5 but for July 7 at 6:41 pm.

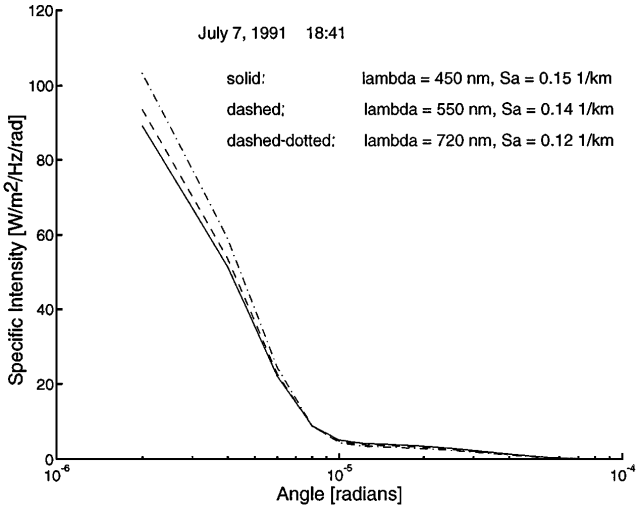

Fig. 12. Calculated specific-intensity functions with scattering coefficients for coarse and fine aerosols together for July 7 at 6:41 pm.

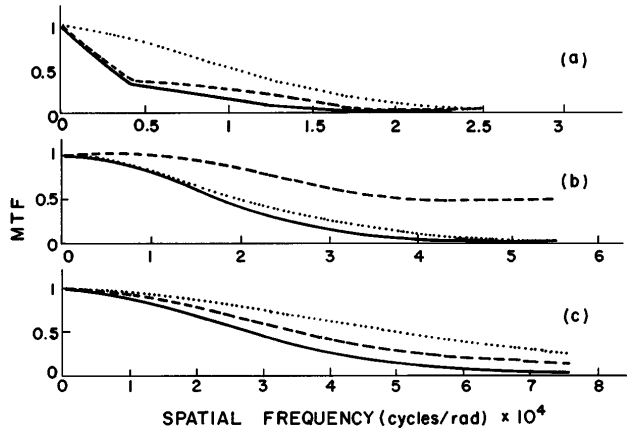

Fig. 13. Overall atmospheric, turbulence, and aerosol MTF's measured with a He–Ne laser (663-nm wavelength). (a) August 18, 1991, 9:35 am; (b) Aug. 13, 1991, 1:10 pm; (c) Aug. 14, 1991, 8:34 pm. Symbols for overall atmospheric, turbulence, and aerosol MTF's as in Figs. 5, 9, and 11.

bulence and practical aerosol MTF's are quite clearly evident, and Ω_c is approximately an order-of-magnitude higher spatial frequency than the bandwidth limitation in Bissonnette's experiment.

An indication of the accuracy of the measurement techniques presented here can be obtained from recent measurements of the effects of forward light scatter by aerosols on atmospheric coherence diameter for both short and long exposures.[34] Using the same techniques as those used here to separate out turbulence and aerosol MTF's, we found that short- (1/1200-s) and long-exposure aerosol MTF's are identical, unlike short- and long-exposure turbulence MTF's, which are not. Since aerosol MTF does not display the time-varying wave-front tilt of turbulence, it is natural to expect no dependence on exposure times (except for time scales associated with the speed of light). The facts that short- and long-exposure aerosol MTF's were identical and that short- and long-exposure turbulence MTF's were not support the method of separating out aerosol and turbulence MTF's developed here.

5. CONCLUSIONS

Even though measured wavelength dependence of overall atmospheric MTF has in the past indicated a strong role for aerosol MTF in limiting image quality through the atmosphere,[28] we believe that our experiments are the first in which the aerosol MTF has been isolated and identified for actual aerosol size *distributions* measured simultaneously in the open atmosphere. The narrower the scattering diagram and the greater the scattering density, the more serious is the image degradation resulting from aerosols. Furthermore, the role played by small-angle particulate scatter in limiting image quality often appears to be more significant than that of turbulence. In general, overall atmospheric MTF was observed to be dominated by aerosol MTF even around midday at approximately 15-m elevation. Since turbulence MTF is very sensitive to elevation, C_n^2 can be expected to be much greater at 1- or 2-m elevation, and turbulence MTF can be expected to be of much greater relative significance at that low level. However, since aerosol size distribution varies little up to the boundary layer, these results at 15-m elevation suggest that imaging through vertical or slant paths is affected very significantly by aerosols and perhaps much more so than by turbulence. In thermal infrared imaging the relative role of aerosol MTF is even greater than in the visible.[35] The lack of wave-front tilt produced by aerosols suggests that aerosol-derived blur is not corrected with adaptive optics. Results here indicate that such blur is often very significant. Hence, aerosol MTF should be taken into account also in adaptive optics imaging. One solution shown to be successful is digital image restoration based on aerosol MTF.[12] The unique shape of the aerosol MTF is critical to such image restoration.[11,36,37] Such restoration can be applied to images already corrected for turbulence with adaptive optics.

Imaging through the atmosphere is much more complicated than imaging with a single wavelength through a path consisting of single-sized aerosols as in controlled experiments in the literature.[30,31] In our case the particulate size distribution is spread over a wide range of particulate radii. Because larger particulates do more scattering, distribution according to particulate optical cross-sectional area is more representative of scattering processes. The latter distribution often peaks for

coarse aerosols at 5–10 μm, depending on climate and weather.[17,32] In the case of imaging through a wide particulate distribution, it is not practical to use a simplified MTF model such as the classical aerosol MTF[4,5] nor to relate the scattering and absorption effects to a certain dominant radius in order to produce an accurate model for the aerosol MTF curve. A practical model for aerosol MTF that considers size distribution (and resulting scattering diagrams and densities) and instrumentation effects is presented elsewhere.[6] The data here support such a practical aerosol MTF model. Indeed, actual calculation of the instrumentation-limited MTF with use of the aerosol and instrumentation data presented here yields MTF curves (Fourier transformations of specific-intensity functions) similar to those measured here for aerosol MTF. Since examples appear in Ref. 6 they are not repeated here. The relatively high aerosol MTF cutoff frequency Ω_c was seen here to be limited by dynamic range rather than by field of view.[6] The data shown here derive from the passive edge-response method and the active method in which the He–Ne laser beam serves as a point object. It should be pointed out, however, that experiments in which C_n^2 is measured as described here but in which overall atmospheric MTF is obtained from simultaneous measurement of bar chart contrast in which first-harmonic contributions only at each discrete spatial frequency are considered also yield similar aerosol MTF results, including comparison with turbulence MTF.[29]

These results suggest that although relatively fast-moving particulates can contribute slightly to scintillation and angle-of-arrival variance compared with turbulence as a result of multipath interference effects,[14,38] slowly varying or relatively static aerosols diffuse and broaden propagation beam widths significantly. The latter particulates appear to be the primary cause of blurring by particulate scatter as described by the aerosol MTF.

Results presented here suggest that aerosol MTF should be considered strongly in system design and in image processing and restoration for imaging through the atmosphere. This has been demonstrated experimentally.[12,36,37]

ACKNOWLEDGMENTS

The assistance of Arnon Karnieli of the Blaustein Desert Research Institute in Sde Boker, Israel, regarding Fig. 3 is greatly appreciated. The authors also thank the Israel Institute for Biological Research for the loan of meteorological equipment. The authors are grateful to D. L. Fried for his constructive comments while he was on a visit during the course of this research. This work is supported partially by the National Council for Research and Development of the Ministry of Science and Technology, Jerusalem, Israel.

REFERENCES

1. D. Sadot, D. Shemtov, and N. S. Kopeika, "Theoretical and experimental investigation of image quality through an inhomogeneous turbulent medium," Waves Random Media **4,** 177–189 (1994).
2. D. L. Fried, "Optical resolution through a random medium for very long and very short exposures," J. Opt. Soc. Am. **56,** 1372–1379 (1966).
3. N. S. Kopeika, "Imaging through the atmosphere for airborne reconnaissance," Opt. Eng. **26,** 1146–1154 (1987).
4. R. F. Lutomirsky, "Atmospheric degradation of electrooptical system performance," Appl. Opt. **17,** 3915–3921 (1978).
5. A. Ishimaru, "Limitations on image resolution imposed by a random medium," Appl. Opt. **17,** 348–352 (1978).
6. D. Sadot and N. S. Kopeika, "Imaging through the atmosphere: practical instrumentation-based theory and verification of aerosol modulation transfer function," J. Opt. Soc. Am. A **10,** 172–179 (1993).
7. E. P. Zege, A. P. Ivanov, and I. L. Katsev, *Image Transfer through a Scattering Medium* (Springer-Verlag, Berlin, 1991).
8. L. Bissonnette, "Imaging through fog and rain," Opt. Eng. **31,** 1045–1052 (1992).
9. D. Sadot and N. S. Kopeika, "Effects of absorption on image quality through a particulate medium," Appl. Opt. **33,** 7107–7111 (1994).
10. R. E. Hufnagel and N. R. Stanley, "Modulation transfer function through turbulent media," J. Opt. Soc. Am. **54,** 52–61 (1964).
11. I. Dror and N. S. Kopeika, "Aerosols and turbulence modulation transfer functions: comparison measurements in the open atmosphere," Opt. Lett. **17,** 1532–1534 (1992).
12. D. Sadot, A. Dvir, I. Bergel, and N. S. Kopeika, "Restoration of thermal images distorted by the atmosphere, based upon measured and theoretical atmospheric modulation transfer function," Opt. Eng. **33,** 44–53 (1994).
13. N. S. Kopeika, I. Kogan, R. Israeli, and I. Dinstein, "Prediction of images propagation quality through the atmosphere: the dependence of atmospheric modulation transfer function on weather," Opt. Eng. **29,** 1427–1438 (1990).
14. D. Sadot and N. S. Kopeika, "Forecasting optical turbulence strength on the basis of macroscale meteorology and aerosols: models and validation," Opt. Eng. **31,** 200–212 (1992).
15. J. Smith, U.S. Army Night Vision Laboratory, Fort Belvoir, Va. (personal communication, 1993).
16. J. Gottlieb, B. Fugel, I. Dror, Z. Y. Offer, and N. S. Kopeika, "Prediction of airborne particle statistics according to weather forecast: concentration and scattering area," Opt. Eng. **34,** 1208–1218 (1995).
17. I. Dror and N. S. Kopeika, "Prediction of particulate size distribution according to weather parameters," in *Atmospheric Propagation and Remote Sensing,* A. Kohnle and W. B. Miller, eds., Proc. Soc. Photo-Opt. Instrum. Eng. **1688,** 123–131 (1992).
18. C. F. Bohren and D. R. Huffman, *Absorption and Scattering of Light by Small Particles* (Wiley, New York, 1983), Chap. 4.
19. J. Canny, "A computational approach to edge detection," IEEE Trans. Pattern Anal. Mach. Intell. **PAMI-8,** 679–698 (1986).
20. A. E. Marble and A. M. Zayezdany, "Adaptive numerical smoothing: an efficient method of conditioning physiological signals," Med. Biol. Eng. Comput. **27,** 171–180 (1989).
21. H. Raidt and D. H. Hohn, "Instantaneous intensity distribution in a focused laser beam at 0.63 μm and 10.6 μm propagating through the atmosphere," Appl. Opt. **14,** 2747–2749 (1975).
22. I. Dror, S. Atar, and N. S. Kopeika, "Prediction of atmospheric extinction coefficient and comparison of transmission measurement methods: black target contrast vs. aerosol scattering calculations," in *Characterization, Propagation, and Simulation of Sources and Backgrounds III,* W. R. Watkins and D. Clement, eds., Proc. Soc. Photo-Opt. Instrum. Eng. **1967,** 331–334 (1993).
23. W. E. K. Middelton, *Vision through the Atmosphere* (U. Toronto Press, Ontario, Canada, 1958).
24. W. C. Malm, "Consideration in the accuracy of a long-path transmissometer," Aerosol Sci. Technol. **14,** 459–471 (1991).
25. R. R. Beland, "Propagation through atmospheric optical turbulence," in *Atmospheric Propagation of Radiation,* F. G. Smith, ed., Vol. 2 of the Infrared and Electrooptical Systems Handbook, J. S. Accetta and D. L. Shumaker, exec. eds. (ERIM, Ann Arbor, Mich., and Society of Photo-Optical Instrumentation Engineers, Bellingham, Wash., 1993), p. 195.

26. E. C. Crittenden, A. W. Cooper, E. A. Milne, G. W. Rodeback, S. H. Kalmback, and R. L. Armstead, "Effects of turbulence on imaging through the atmosphere," in *Optical Properties of the Atmosphere,* R. C. Sepucha, ed., Proc. Soc. Photo-Opt. Instrum. Eng. **142,** 130–134 (1978).
27. D. L. Fried, "Anisoplantism in adaptive optics," J. Opt. Soc. Am. **72,** 52–81 (1982).
28. N. S. Kopeika, S. Solomon, and Y. Gencay, "Wavelength variation of visible and near-infrared resolution through the atmosphere: dependence on aerosol and meteorological conditions," J. Opt. Soc. Am. **71,** 892–901 (1981).
29. I. Dror and N. S. Kopeika, "Cutoffs of overall atmospheric MTF," in *Propagation Engineering: Fourth in a Series,* L. Bissonnette and W. Miller, eds., Proc. Soc. Photo-Opt. Instrum. Eng. **1487,** 192–202 (1991).
30. Y. Kuga and A. Ishimaru, "Modulation transfer function and image transmission through randomly distributed spherical particles," J. Opt. Soc. Am. A **2,** 2330–2335 (1985).
31. P. Donelli, P. Bruscaglioni, A. Ismaelli, and G. Zaccanti, "Experimental validation of a Monte Carlo procedure for the evaluation of the effect of a turbid medium on the point spread function of an optical system," J. Mod. Opt. **38,** 2189–2201 (1991).
32. Y. J. Kim, H. Sievering, and J. F. Boatman, "Airborne measurement of atmospheric aerosol particle in the lower troposphere over the central United States," J. Geophys. Res. **93,** 631–644 (1988).
33. N. S. Kopeika and D. Sadot, "Imaging through the atmosphere: practical instrumentation-based theory and verification of aerosol modulation transfer function: reply to comment," J. Opt. Soc. Am. A **12,** 1017–1023 (1995).
34. D. Sadot, A. Melamed, N. Dinur, and N. S. Kopeika, "Effects of aerosol forward scatter on long and short exposure atmospheric coherence diameter," Waves Random Media **4,** 482–498 (1994).
35. D. Sadot and N. S. Kopeika, "Thermal imaging through the atmosphere: atmospheric MTF theory and verification," Opt. Eng. **33,** 880–887 (1994).
36. D. Sadot, S. R. Rotman, and N. S. Kopeika, "Comparison between high-resolution restoration techniques of atmospherically distorted images," Opt. Eng. **34,** 144–153 (1995).
37. D. Sadot, G. Lorman, R. Lapardon, and N. S. Kopeika, "Restoration of thermal images distorted by the atmosphere using predicted atmospheric modulation transfer function," Infrared Phys. Technol. **36,** 565–576 (1995).
38. A. D. Sarma and R. J. Hill, "Effect of blowing snow and ground blizzards on millimeter wave scintillation spectra," Int. J. Infrared Millimeter Waves **12,** 997–1022 1991.